

Multibeam Raman amplification of a finite-duration seed in a short distance

Y G Chen(陈雨谷), Y Chen(陈勇), S X Xie(谢善秀), N Peng(彭娜), J Q Yu(余金清), and C Z Xiao(肖成卓)
Citation: Chin. Phys. B, 2021, 30 (**10**): 105202. DOI: 10.1088/1674-1056/ac0521
Journal homepage: http://cpb.iphy.ac.cn; http://iopscience.iop.org/cpb

What follows is a list of articles you may be interested in

Tests of the real-time vertical growth rate calculation on EAST

Na-Na Bao(鲍娜娜), Yao Huang(黄耀), Jayson Barr, Zheng-Ping Luo(罗正平), Yue-Hang Wang(汪悦航), Shu-Liang Chen(陈树亮), Bing-Jia Xiao(肖炳甲), David Humphreys
Chin. Phys. B, 2020, 29 (**6**): 065204. DOI: 10.1088/1674-1056/ab84da

Rayleigh-Taylor instability at spherical interfaces of incompressible fluids

Hong-Yu Guo(郭宏宇), Li-Feng Wang(王立锋), Wen-Hua Ye(叶文华), Jun-Feng Wu(吴俊峰), Ying-Jun Li(李英骏), Wei-Yan Zhang(张维岩)
Chin. Phys. B, 2018, 27 (**2**): 025206. DOI: 10.1088/1674-1056/27/2/025206

Rayleigh-Taylor instability of multi-fluid layers in cylindrical geometry

Hong-Yu Guo(郭宏宇), Li-Feng Wang(王立锋), Wen-Hua Ye(叶文华), Jun-Feng Wu(吴俊峰), Wei-Yan Zhang(张维岩)
Chin. Phys. B, 2017, 26 (**12**): 125202. DOI: 10.1088/1674-1056/26/12/125202

Magneto-Rayleigh–Taylor instability in compressible Z-pinch liner plasmas

Xue Yang(杨学), De-Long Xiao(肖德龙), Ning Ding(丁宁), Jie Liu(刘杰)
Chin. Phys. B, 2017, 26 (**7**): 075202. DOI: 10.1088/1674-1056/26/7/075202

Preparation and structural properties of thin carbon films by very-high-frequency magnetron sputtering

Ming-Wei Gao(高明伟), Chao Ye(叶超), Xiang-Ying Wang(王响英), Yi-Song He(何一松), Jia-Min Guo(郭佳敏), Pei-Fang Yang(杨培芳)
Chin. Phys. B, 2016, 25 (**7**): 075202. DOI: 10.1088/1674-1056/25/7/075202

Multibeam Raman amplification of a finite-duration seed in a short distance*

Y G Chen(陈雨谷)[1], Y Chen(陈勇)[1], S X Xie(谢善秀)[1], N Peng(彭娜)[1], J Q Yu(余金清)[1], and C Z Xiao(肖成卓)[1,2,†]

[1] *Key Laboratory for Micro-/Nano-Optoelectronic Devices of Ministry of Education, School of Physics and Electronics, Hunan University, Changsha* 410082, *China*

[2] *Collaborative Innovation Center of IFSA (CICIFSA), Shanghai Jiao Tong University, Shanghai* 200240, *China*

(Received 20 April 2021; revised manuscript received 22 May 2021; accepted manuscript online 26 May 2021)

A new scheme of multibeam Raman amplification (MRA) is proposed in virtue of the collective mode by sharing a common scattered light. Multiple laser beams can provide a higher growth rate, but the overlapping region limits the amplification length. We suggest to use a finite-duration seed to facilitate MRA in a short distance. Through two-dimensional particle-in-cell simulations, we find that two-beam Raman amplification has a much higher growth rate than that of single-beam one. This growth rate depends on the initial seed amplitude, electron temperature, and seed duration. An empirical criterion, $\gamma_0\tau_c = 1$, where γ_0 is the theoretical growth rate of MRA, is used to choose a proper duration for a higher growth rate. After a total amplification length of 320 μm, the two-beam Raman amplification shows nonlinear features of pulse compression and a bow-shape wave front, indicating that the amplification has finally entered the self-similar regime.

Keywords: multibeam Raman amplification, growth rate, finite-duration

PACS: 52.38.–r, 52.65.–y **DOI:** 10.1088/1674-1056/ac0521

1. Introduction

Laser intensity is limited to the optical intensity of gratings, which is a critical issue for chirped pulse amplification (CPA) technology,[1,2] due to damage threshold. Therefore, amplifiers based on plasma medium, whose tolerant intensity is about 10^4–10^5 times of solid-state optics,[3] was proposed. Malkin, Shvets, and Fisch proposed the basic principle of compressing the laser beam to highly overcritical power via stimulated Raman backscattering (SRBS).[4–8] It is based on the three-wave interaction, in which the pump wave, backpropagating seed pulse, and Langmuir wave should satisfy the phase matching condition. The seed pulse absorbs the power of the pump wave and gets an intensity much higher than the pump wave in the nonlinear stage of SRBS, so it is called backward Raman amplification (BRA).[4,6,9] This scheme will lead to high-intensity seed pulse even in the exawatt regime by using plasma as the medium.[4,6,10–13] The BRA concept has been theoretically[4,6,14–18] and experimentally[19–23] explored a lot.

Collective modes of multibeam stimulated Raman scattering (SRS), which have higher growth rates than the single beam one, have been discovered for many years, and they are hazardous to the inertial confinement fusion.[16,17,24,25] However, this feature may facilitate Raman amplification. The idea of using multiple laser beams in Raman amplifier was first proposed by Balakin *et al.*[26] to suppress noise and enhance focusability. Their analysis was limited to paraxial approximation where the beam angles are only few degrees, so it is actually a modified BRA. In our consideration, multiple laser beams overlap with large incidence angles as seen in laser facilities such as National Ignition Facility (NIF).[27] Under that circumstances, we can use the advantage of a large number of laser beams to provide a higher Raman growth rate. But one should also note that due to overlapping the amplification length is finite. Typical amplification time, $w/c\sin\varphi$, is only about 2–3 picoseconds, where w is the beam width, φ is the angle of incidence, and c is the speed of light. Therefore, how to achieve higher seed intensity in such a short distance is one of the main issues in the multibeam Raman amplification (MRA).

In this paper, we demonstrate proof-of-concept numerical studies by focusing on the simplest case of two-beam amplification. Geometry of MRA and its linear growth rate are studied first. We use a collective mode by sharing a common scattered light to accomplish MRA, and its growth rate is proportional to the square root of the beam number. Unlike the conventional BRA regime, finite-duration seed is used here to take advantage of the growth of the initial seed pulse. Since a second pulse (the Raman Stokes wave) trailing the original seed pulse grows from zero amplitude, if the seed duration is negligible, it will take a considerable time for the second pulse to reach the unchanged initial seed amplitude. While

*Project supported by the Strategic Priority Research Program of Chinese Academy of Sciences (Grant No. XDA25050700), the National Natural Science Foundation of China (Grant No. 11805062), Science Challenge Project (Grant No. TZ2016005), and Natural Science Foundation of Hunan Province, China (Grant Nos. 2020JJ5029 and 2020JJ5031), and the Project of Science and Technology on Plasma Physics Laboratory (Grant No. 6142A04190111).

†Corresponding author. E-mail: xiaocz@hnu.edu.cn

© 2021 Chinese Physical Society and IOP Publishing Ltd

using finite seed duration, the original seed pulse can directly gain energy from the pump beams instead of waiting for the growth of the second pulse. We find that the real-amplitude growth rate is a function of the initial seed amplitude, electron temperature, and seed duration. For a fixed seed amplitude, the growth rate saturates at $\gamma_0\tau_c = 1$, where γ_0 is the linear growth rate and τ_c is the critical seed duration. This formula gives us a proper choice of seed duration for amplification. We also find by performing three-wave coupling simulations and two-dimensional particle-in-cell (PIC) simulations that the growth rate of two-beam amplification is much larger than that of the single-beam amplification. After the initial exponential growth, the two-beam amplification enters the nonlinear stage more rapidly and shows features of pulse compression and a bow-shape wave front, which indicates the amplification has entered the self-similar (π-pulse) regime.

The paper is organized as follows. In Section 2, we present a brief derivation of multibeam linear growth rate based on the full wave coupling equations. Simulation models are discussed in Section 3. In Sections 4 and 5, we show how finite-duration seed pulse can gain energy from two pump beams in a short distance through three-wave coupling simulations and 2D PIC simulations at the linear and nonlinear stages. We summarize the MRA scheme in Section 6.

2. Linear growth rate of MRA

In the conventional BRA scheme, pump laser (ω_0, k_0) and seed pulse (ω_s, k_s) are coupled by Langmuir wave $(\omega_{l\omega}, k_{l\omega})$ through phase-matching condition: $\omega_0 = \omega_s + \omega_{l\omega}$ and $k_0 = k_{l\omega} - k_s$, as shown in Figs. 1(a) and 1(c). The physics can be described by the three-wave coupling equations of fluid limit[4,28]

$$\left(\frac{\partial^2}{\partial t^2} - c^2\nabla^2 + \omega_{pe}^2\right)\boldsymbol{A}_0 = -\omega_{pe}^2\tilde{n}_e\boldsymbol{A}_s, \tag{1}$$

$$\left(\frac{\partial^2}{\partial t^2} - c^2\nabla^2 + \omega_{pe}^2\right)\boldsymbol{A}_s = -\omega_{pe}^2\tilde{n}_e\boldsymbol{A}_0, \tag{2}$$

$$\left(\frac{\partial^2}{\partial t^2} + \omega_{pe}^2 - 3v_e^2\nabla^2\right)\tilde{n}_e = \frac{n_0e^2}{m_e^2c^2}\nabla^2(\boldsymbol{A}_0\cdot\boldsymbol{A}_s), \tag{3}$$

where $\boldsymbol{A}_s$ and $\boldsymbol{A}_0$ are the vector potentials of the scattered light wave and the pump wave, respectively, and $\tilde{n}_e$ is the electron density fluctuation of the Langmuir wave. In addition, ω_{pe} is the plasma frequency, v_e is the electron thermal velocity, e and m_e are the charge and mass of electron.

Assuming $A_0 =$ const. and performing Fourier transform on Eqs. (2) and (3), we can get the linear dispersion relation. The growth rate of BRA in homogeneous plasmas is readily obtained by solving the dispersion relation[29]

$$\gamma_{BRA} = \frac{k_{l\omega}v_{os}}{4}\left[\frac{\omega_{pe}^2}{\omega_{l\omega}(\omega_0 - \omega_{l\omega})}\right]^{1/2}, \tag{4}$$

where $v_{os} = eA_0/m_ec$ is the electron oscillation velocity.

The linear growth rate of multibeam Raman scattering[16,30,31] can be derived from those equations as well just by considering $\boldsymbol{A}_0$ as a superposition of multiple laser fields. The process to get the dispersion relation is similar to the single-beam one (see detailed derivation in Ref. [16]). The difference is that MRA relies on collective modes that geometrically symmetric pump lasers share a common scattered light.[16,25,32] The geometry of a two-beam amplification is shown in Figs. 1(b) and 1(d) where a seed pulse propagates along the bisector of two pump wave vectors.

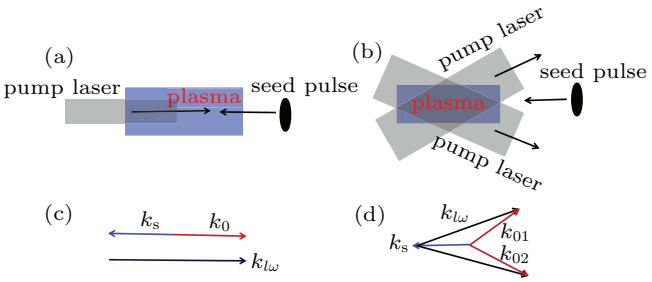


Fig. 1. (a), (b) are the diagram of single-beam amplification and two-beam amplification, respectively. Wave number matching condition of (c) single-beam amplification, where the scattered light is opposite to the direction of the pump laser; and (d) two-beam amplification, where the geometrically symmetric pump lasers share a common scattered light.

In the MRA, the maximum growth occurs when the seed pulse is resonant with all multiple pump lasers through symmetric and obliquely propagating Langmuir waves,

$$\boldsymbol{k}_s = \boldsymbol{k}_{0i} - \boldsymbol{k}_{l\omega_i}, \quad i = 1, \ldots, N. \tag{5}$$

The linear growth rate of Raman amplification under N symmetric laser beams is given by[16]

$$\gamma_0^2 = N\gamma_{BRA}^2\langle\cos^2\varphi\rangle, \tag{6}$$

where $\langle\cos^2\varphi\rangle = \frac{1}{N}\sum_{i=1}^{N}\cos^2\varphi_{0i}$ is the average polarization factor. In the two-beam Raman amplification, Eq. (5) gives $k_{l\omega} = \sqrt{k_{01}^2 + k_s^2 + 2k_{01}k_s\cos\phi}$, where ϕ is the incidence angle of the pump lasers. Usually, the Langmuir wavenumber in the single-beam amplification, $k_{l\omega} = k_0 + k_s$, is larger than that in the two-beam amplification within a factor of 2. $\langle\cos^2\varphi\rangle = 1$ is assumed in the remainder part of two-beam amplification. It is also obvious that the multibeam growth rate is nearly $\sqrt{N}$ times of the single-beam one.

3. Simulation models

The full-wave Eqs. (1)–(3) are usually simplified to the first order equations by using envelope approximation. But for a large angle of incidence, the Laplace operator ∇^2 cannot be separated via paraxial approximation.[26] One must solve the full-wave equations to capture the correct dynamics in the transverse direction.

Here, we use two simulation models. First, by totally neglecting the transverse behaviors, the first order three-wave coupling equations are derived along the symmetric axis as

$$\begin{aligned}(\partial_t + V_{0x}\partial_x)a_0 &= -\Gamma a_1 a_2,\\ (\partial_t + V_{\rm s}\partial_x)a_1 &= \Gamma a_0 a_2^*,\\ (\partial_t + V_{l\omega x}\partial_x)a_2 &= \Gamma a_0 a_1^*,\end{aligned} \tag{7}$$

where a_0, a_1, and a_2 are envelopes of the pump laser, seed pulse, and Langmuir wave, respectively. $V_{0x} = k_{0x}c^2/\omega_0$, $V_{\rm s} = -k_{\rm s}c^2/\omega_{\rm s}$, and $V_{l\omega x} = 3k_{l\omega x}v_{\rm e}^2/\omega_{l\omega}$ are the group velocities of the three waves along the x-axis, and $\gamma_0 = a_0\Gamma$ is the linear growth rate of MRA. Actually, this model is very accurate for describing BRA, but we use it to capture the rough behavior in the longitudinal direction just by substituting $\gamma_{\rm BRA}$ with γ_0. We have solved the three-wave coupling equations numerically to obtain the linear growth pattern of Raman amplification resulting from different seed durations.

Further, a more radical model, i.e., PIC simulation, is used to study the whole linear and nonlinear stages of two-beam amplification. 2D PIC simulations via a full three-dimensional, relativistic PIC code EPOCH[18,33,34] are performed.

The simulation parameters are as follows. We specify the wavelength of the pump laser $\lambda_{\rm pump} = 800.0$ nm with an intensity of 2.0×10^{14} W/cm^2. The seed pulse is a Gaussian beam with $\lambda_{\rm seed} = 888.9$ nm, and the full width at half maximum of the seed amplitude is 8 μm. The amplification length for each case is 320 μm and the box width is 80 μm. The entire simulation box is filled with uniform plasmas of density $0.01n_{\rm c}$ ($n_{\rm c}$ corresponds to the critical density of the pump laser), buffered by vacuum regions of 10 μm on both sides of longitudinal direction. The electron temperature is 10 eV and the ions are set to be immobile. The transverse boundary condition is set to be open boundary condition in order to prohibit artificial perpendicular scatterings.[25] When the pump lasers fill in the simulation box, the seed laser is incident from the right hand side of the simulation box. There are 80 particles in each cell and the spatial resolution is 0.04 μm/cell.

The schematic of single-beam Raman amplification is shown in Figs. 1(a) and 1(c), where the pump laser is incident from the left of the simulation box and the entire simulation time is 2400 fs. The geometry for two-beam Raman amplification is shown in Figs. 1(b) and 1(d), where two plane pump lasers are injected from the upper and lower boundaries of the simulated box with a same incidence angle. The entire simulation time is 1600 fs. The duration of the seed pulse is changed in cases.

4. Amplification at the linear stage

4.1. Real-amplitude growth rate

We measure the real-amplitude growth rate of the amplification, which shows the growth of the maximum seed amplitude. As shown in Figs. 7(b) and 8(b), the maximum amplitudes of the seed pulse $A_{\rm seed}$ are extracted from the simulations and we plot $\log(A_{\rm seed}/A_{\rm seed0})$ as a function of time, where $A_{\rm seed0}$ is the amplitude of the initial seed pulse. The real-amplitude growth rate is thus obtained through a linear fitting over time. Note that the real-amplitude growth rate is not exactly equal to the theoretical growth rates discussed in Section 2.

Figure 2 shows the comparison of the theoretical growth rates and the real-amplitude growth rates with different initial seed amplitudes, electron temperatures, and incidence angles of two pump beams from PIC simulations. The pump intensity is 2.0×10^{14} W/cm^2, while the seed intensity increases from 5.0×10^{12} W/cm^2 to 2.0×10^{14} W/cm^2. The theoretical growth rate (black curve, evaluated from Eq. (6)) decreases with the increase of the incidence angle since the Langmuir wavenumber $k_{l\omega}$ is decreasing. The tendency of real-amplitude growth rates (marked lines) is consistent with the theoretical results very well.

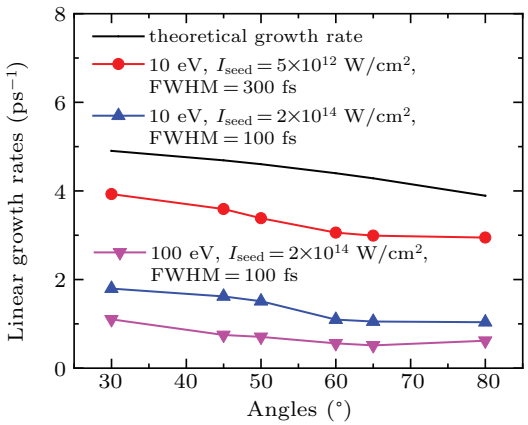


Fig. 2. Theoretical and real-amplitude growth rates of two-beam amplification as a function of incidence angle at different original seed intensities and plasma temperatures. The intensity of both pump lasers is 2.0×10^{14} W/cm^2.

It is observed that the real-amplitude growth rate strongly depends on the initial seed amplitude. When the seed amplitude is weak enough, compared to the pump intensity, the real-amplitude growth rate is close to the theoretical one as verified by the red-dotted curve. As the seed amplitude increases to the pump level, the effect of the seed amplitude on the growth rate cannot be neglected. Thus, the growth rate decreases by nearly a factor of 2. Landau damping also plays an important role in the growth rate. As the temperature goes up, the real-amplitude growth rate decreases as shown in the blue-up-triangle curve and purple-down-triangle curve.

4.2. Finite-duration seed to facilitate MRA in a short distance

For mulitbeam Raman amplification with large incidence angle, amplification proceeds in a finite length on the order of beam width. Therefore, conventional scheme of using enough long amplification length is not appropriate for MRA. Here, we use a finite-duration seed to achieve higher seed intensity.

As we know, analytic solutions of Eq. (7) at the linear stage ($a_0 = \text{const.}$) can be obtained through Green functions.[34–36] Assuming the initial values $a_2(x,0) = 0$ and $a_1(x,0) = a_{10}\,\mathrm{e}^{-x^2/D^2}$, the spatio-temporal evolution of the seed pulse is[35]

$$a_1(x,t) = a_1(x+ct,0) + \int^x G(x-x',t)a_1(x',0)\,\mathrm{d}x', \quad (8)$$

and the Green function is

$$G(x,t) = \frac{\gamma_0}{c}\sqrt{\frac{-x}{ct+x}}I_1(\xi)\Theta\left(t+\frac{x}{c}\right), \quad (9)$$

where $I_1(x)$ and $\Theta(x)$ are the first order modified Bessel function and Heaviside step function, respectively, and $\xi = 2(\gamma_0/c)\sqrt{-x(ct+x)}$. If the initial seed is short enough, compared with the Raman length, i.e. $D \ll c/\gamma_0$, Eq. (8) reduces to

$$a_1(x,t) \approx a_1(x+ct,0) + a_{10}\gamma_0\tau\sqrt{\frac{-x}{ct+x}}I_1(\xi), \quad (10)$$

where τ is the seed duration (full width at half maximum).

The solution involves an initial seed pulse propagating with the speed of light (the first term) and a pumped pulse excited by the resonant interaction (the second term). The maximum growth of the pumped pulse occurs at $x = -ct/2$, growing with the homogeneous growth rate γ_0. Nevertheless, the real-amplitude growth rate is defined by the growth of the maximum of $a_1(x,t)$. If τ is negligible, not until the maximum of the pumped pulse reaches a_{10}, the real-amplitude growth rate remains null. The time t_0 to reach the initial seed amplitude is approximated by $I_1(\gamma_0 t_0) = 1/\gamma_0\tau$, which increases logarithmically as τ vanishes. When τ is finite, both two terms contribute to the growth of the seed pulse, so the real-amplitude growth rate is a function of duration, $\gamma = \gamma(\tau)$.

To demonstrate this effect, we numerically solve Eq. (7) and plot evolutions of the seed pulse with finite durations in Fig. 3. Here the pump and seed pulse intensities are 2.0×10^{14} W/cm^2 and 2.0×10^{12} W/cm^2, respectively, and this corresponds to a two-beam growth rate $\gamma_0 = 4.90$ ps^{-1}. When the initial seed duration is 48 fs, a fast-growing second pulse gradually appears at the tail of the original seed and it broadens over time as shown in Fig. 3(a). At $t \approx 1600\omega_0^{-1} = 679$ fs, the second pulse catches up the original seed, which is accordant with the estimation, $t_0 \approx 629$ fs. The leading pulse propagates at a speed of 2.944×10^8 m/s and it has a small growth rate of 0.690 ps^{-1}; while the second pulse propagates at a speed of 1.677×10^8 m/s and it has a growth rate of 4.166 ps^{-1} close to the theoretical growth rate. When the duration is long enough, $\tau = 573$ fs in Fig. 4(b), the leading pulse keeps its original envelope shape as the amplitude grows. The amplitude maximum propagates at a speed of 1.940×10^8 m/s and the real-amplitude growth rate is 4.277 ps^{-1}. Since it grows from the original seed pulse, it can achieve higher amplitude in the same amplification length.

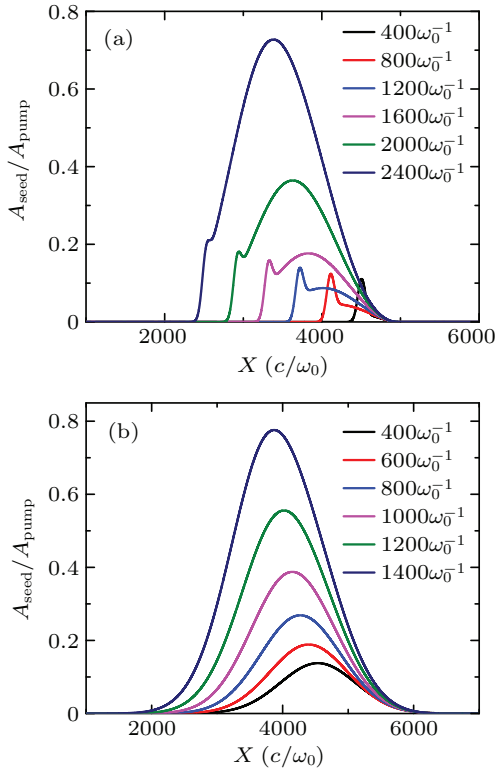


Fig. 3. Evolution of seed amplification at various times through three-wave coupling simulations. The seed pulse has a short duration of 48 fs in (a) and a long duration of 573 fs in (b). The seed laser intensity is 2.0×10^{12} W/cm^2, and the pump laser intensity is 2.0×10^{14} W/cm^2.

Next, we apply the idea to study the MRA in multidimensions and compare the efficiencies of single-beam amplification and two-beam amplification. Figure 4 shows the evolution of the seed envelopes along the center line of the simulation box in a 2D single-beam Raman amplification process. The intensities of the pump laser and seed pulse are both 2.0×10^{14} W/cm^2, and the duration of the seed pulse is (a) 30 fs and (b) 100 fs, respectively. As the seed pulse enters the simulation box, its normalized amplitude is $A_{\rm seed} = 0.0103$ at 1.42 ps. A second pulse forms later and broadens over time. After passing through 320 μm, the amplitude of the seed pulse is almost unchanged, $A_{\rm seed} = 0.0108$ at $t = 2.22$ ps, since it takes so much time for the second pulse to be amplified from noise. While in Fig. 4(b), the seed pulse is amplified rapidly with only one peak. It shows good agreement with the analyses of the three-wave coupling equations.

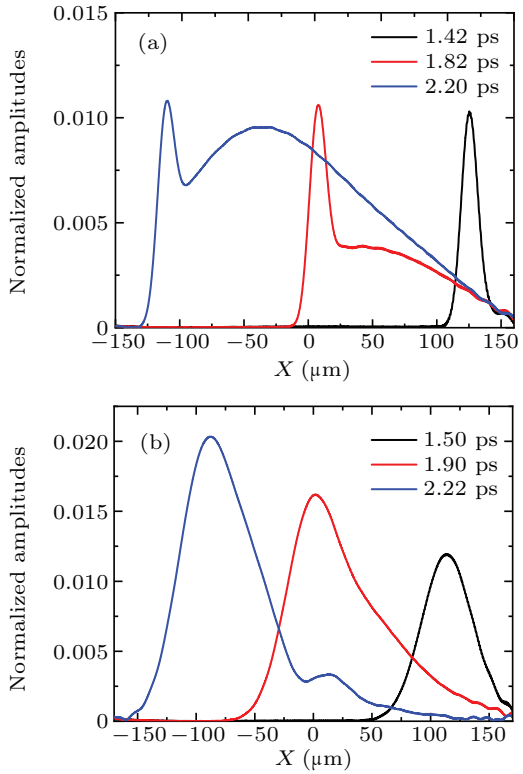


Fig. 4. (a) Time history of seed pulse envelope at $y = 0$ with the pulse duration 30 fs. (b) Time history of seed pulse envelope at $y = 0$ with the pulse duration 100 fs. The intensity of each pump laser and seed laser pulse is the same, 2.0×10^{14} W/cm^2. The seed laser pulse enters the simulation box at (a) $t = 1.23$ ps and (b) $t = 1.27$ ps, and stops the amplification at $t = 2.22$ ps.

Figure 5 shows the evolution of the seed envelopes along the center line of the simulation box in a two-beam Raman amplification with an incidence angle of 30°. The duration of the seed pulse is (a) 30 fs and (b) 100 fs, respectively, and the intensity of the pump lasers and seed pulse is 2.0×10^{14} W/cm^2. In Fig. 5(a), the duration of the seed pulse is broadened first and then compressed, accompanying with the amplitude increased rapidly. At the end of the simulation, $t = 1.6$ ps, the seed amplitude increases to $A_{\text{seed}} = 0.0269$, which is 2.36 times of the initial amplitude. In the whole simulation, we observe the formation of the second pulse, but the second pulse is growing fast even when the duration is only 30 fs. In Fig. 5(b), there is a small broadening in the seed pulse, and the amplitude is increased more rapidly than that in Fig. 5(a). No second pulse is formed in this case.

By comparing the two amplification schemes, we find that the real-amplitude growth rate in two-beam amplification is much larger than the single-beam one. For further interpretation we plot the real-amplitude growth rate as a function of the seed duration in Fig. 6. The real-amplitude growth rate of the single-beam amplification and two-beam amplification is very low when the duration is short, and it increases with the duration. It finally saturates at a level of 1.10 ps^{-1} (2.34 ps^{-1}) in the single-beam (two-beam) amplification, however, this level is lower than the theoretical growth rate, $\gamma_0 = 3.57$ ps^{-1} ($\gamma_0 = 4.90$ ps^{-1}). The discrepancy is due to the choice of a higher initial seed amplitude ($I_{\text{seed0}} = I_{\text{pump}}$) and the increase of Landau damping by heating the plasma, as interpreted in Fig. 2. In addition, we find that the real-amplitude growth rate of the two-beam amplification is nearly 2 times of that of the single beam amplification, which is a little bit larger than the theoretical prediction, $\sqrt{2}$, evaluated from Eq. (6). The reason is that the real-growth rate of the two-beam amplification increases faster than the single-beam one, when both amplifications are under the theoretical growth rate. This behavior is verified by our three-wave coupling simulations. Therefore, we find that the seed pulse grows much faster in the two-beam amplification.

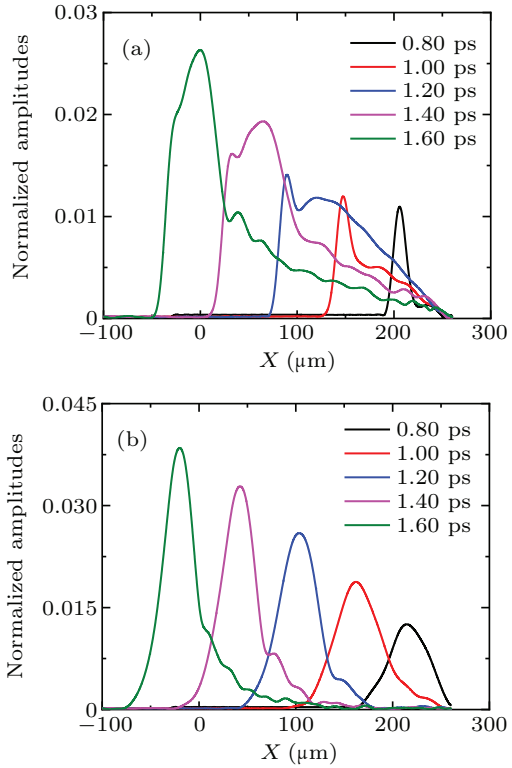


Fig. 5. (a) Time history of seed pulse envelope at $y = 0$ with the pulse duration 30 fs. (b) Time history of seed pulse envelope at $y = 0$ with the pulse duration 100 fs. The intensity of each pump laser and seed laser pulse is 2.0×10^{14} W/cm^2. The seed laser pulse enters the simulation box at (a) $t = 0.615$ ps and (b) $t = 0.65$ ps, and stops the amplification at $t = 1.60$ ps.

Figure 6 also helps us to choose a proper seed duration to facilitate the MRA with higher growth rate. We summarize the rules of growth by an empirical criterion

$$\gamma_0 \tau_c = 1, \tag{11}$$

under a fixed initial seed amplitude. Below the critical duration, the real-amplitude growth rate gradually increases, while above that the growth rate begins to saturate. We have verified the criterion from our PIC simulations that $\tau_c = 280$ fs for the single-beam amplification is close to the saturation point of black line in Fig. 6, $\tau \approx 250$ fs, and $\tau_c = 200$ fs for the two-beam amplification is just the saturation point of red line in

Fig. 6, $\tau \approx 200$ fs. Due to the higher growth rate, the two-beam amplification has an advantage of choosing a much shorter duration.

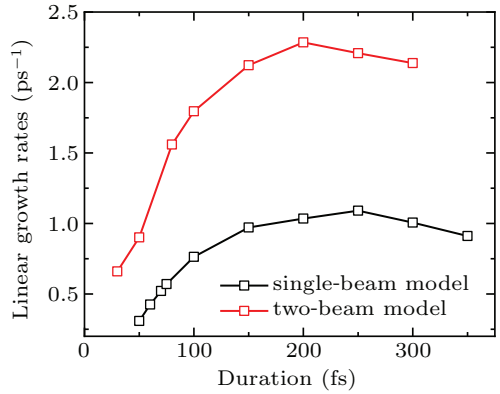


Fig. 6. The simulated growth rates of the seed pulse as a function of seed duration. Black line is single-beam model, and red line is two-beam model with the incidence angle of seed laser being 30°. In the two models, the intensity of each pump laser and seed laser pulse is 2.0×10^{14} W/cm^2.

At the critical duration, the seed pulse has both a higher growth rate and initially shorter duration. Its shape is well preserved in the whole amplification process without triggering an apparent second pulse tailing behind the initial seed pulse. Thus, it helps the seed to gain more energy in a finite amplification length.

5. Amplification at the nonlinear stage

The above analyses are based on the linear amplification where the amplitude increases exponential with time. However, when the seed amplitude is large enough that the pump depletion cannot be ignored, amplification enters the nonlinear stage. Pulse compression is a key character at the nonlinear stage, and it leads the amplification into a self-similar (or π pulse) regime, where the amplitude of the seed pulse increases linearly with time while the seed duration decreases linearly with time. In this section, we show how two-beam amplification enters the nonlinear stage in a finite amplification length of 320 μm and the effect of finite duration on the nonlinear amplification.

The spatio-temporal evolution of the seed amplitude in the single-beam amplification is shown in Fig. 7(a). The initial seed duration is 100 fs and other parameters are mentioned above. The growth factor $(\log(A_{\text{seed}}/A_{\text{seed0}}))$ reflecting the evolution of the maximum amplitude is shown in Fig. 7(b), and it is find that the amplitude of the seed pulse increases exponentially in the whole amplification process, which indicates that the single-beam amplification is still in the linear stage. At the end of the simulation the amplitude of the seed pulse is increased to $A_{\text{seed}} = 0.0203$, which is 1.845 times of the original seed amplitude. The spatio-temporal evolution shows that no pulse compression is observed at this stage, though the seed has already passed 320 μm.

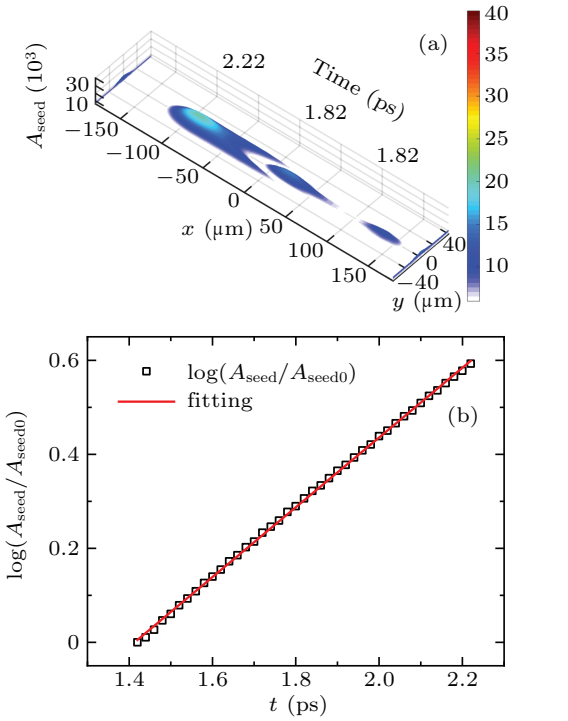


Fig. 7. (a) Evolution of seed amplification at various time. The duration of the seed pulse is 100 fs, and the intensity of each pump laser and seed pulse is 2.0×10^{14} W/cm^2. The seed laser pulse enters the simulation box at $t = 1.27$ ps, and stops the amplification at $t = 2.22$ ps. The amplitude in z-axis is 1000 times its initial amplitude. (b) Growth of the maximum seed pulse amplitude in the logarithmic scale, and its linear curve fitting.

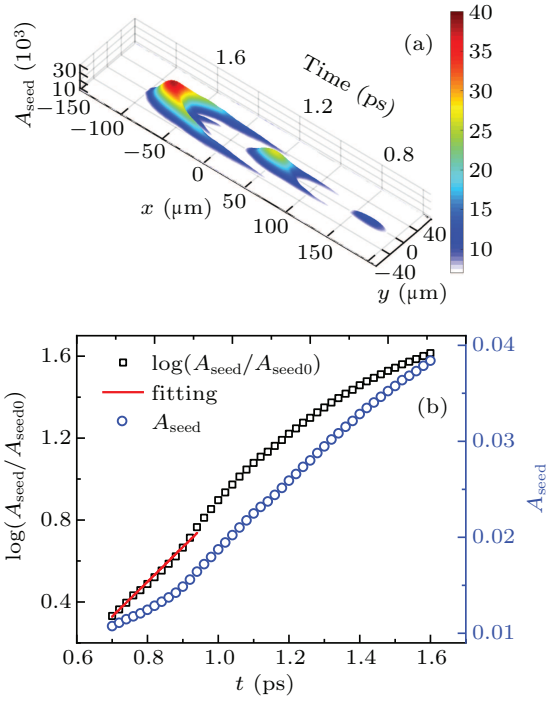


Fig. 8. (a) Evolution of seed amplification at various time. The duration of the seed pulse is 100 fs, and the intensity of each pump laser and seed laser pulse is 2.0×10^{14} W/cm^2. The seed laser pulse enters the simulation box at $t = 0.65$ ps, and stops the amplification at $t = 1.6$ ps. The amplitude in z-axis is 1000 times its initial amplitude. (b) Growth of the maximum seed pulse amplitude in the logarithmic scale, and its linear curve fitting.

Next, we study the nonlinear evolution of the two-beam

amplification. Two pump laser beams are incident from y_{max} and y_{min} with an incidence angle of 30° and the seed duration is 100 fs. Other parameters are the same as the previous ones. The spatio-temporal evolution of the seed amplitude at various time is shown in Fig. 8(a). After interaction, the intensity of the seed pulse increases to $A_{seed} = 0.0384$, which is 3.46 times the initial amplitude of the seed pulse. Figure 8(b) shows the growth of the maximum seed amplitude in logarithmic scale (black dots) and in linear scale (blue dots). It is clearly shown that exponential growth lasts for only 240 fs, from 0.7 ps to 0.94 ps, and its duration is broadening until the amplitude reaches $A_{seed} = 0.0165$. When $t > 0.94$ ps, the seed pulse enters the nonlinear stage, where the seed amplitude increases linearly with time, accompanying with a pulse compression as seen in Fig. 8(a). In addition, the pulse has reformed to a bow shape, which is also a nonlinear feature of Raman amplification. These nonlinear features indicate that the amplification has come into a self-similar regime. Thus, we conclude that the seed pulse enters the nonlinear stage much faster in two-beam amplification than in single-beam amplification due to higher growth rate.

At last, we discuss the effect of duration on the nonlinear amplification. To achieve a higher intensity, the initial seed intensity is increased to 2.0×10^{15} W/cm^2. Two different seed durations are presented in Fig. 9, i.e., (a) 100 fs, (b) 50 fs, and (c) 50 fs. At the end of the simulation, $t = 1.6$ ps, the seed amplitude in Figs. 9(a) and 9(b) grows to $A_{seed} = 0.0541$ and $A_{seed} = 0.0607$, 1.59 times and 1.79 times of the initial seed amplitude ($A_{seed0} = 0.034$), respectively. In Fig. 9(c), when further increasing the pump intensity to 4.0×10^{14} W/cm^2, the seed pulse grows to $A_{seed} = 0.085$, which is 2.46 times the initial seed laser amplitude. Due to the choice of finite duration to facilitate MRA, both of the final amplitudes are higher than the cases before. When the initial seed intensity is high enough, we find that larger seed power (larger duration) is not friendly in keeping the pulse shape as shown in Fig. 9(a) where multiple peaks occur in the seed pulse. While small seed duration helps maintain the pulse shape due to high growth rate and slight wavebreaking. Also, an obvious bow shape of the seed pulse is formed. Besides, we observe that the transverse scale of the pumped pulse is getting larger in the nonlinear stage, since the Langmuir waves excited by the two beams are obliquely propagating as shown in Fig. 1(b). This effect may enhance the efficiency of energy transfer and is good for the subsequent focusing stage. The comparison suggests that a proper short duration without triggering the second pulse can result in higher amplification intensity and better output pulse shape.

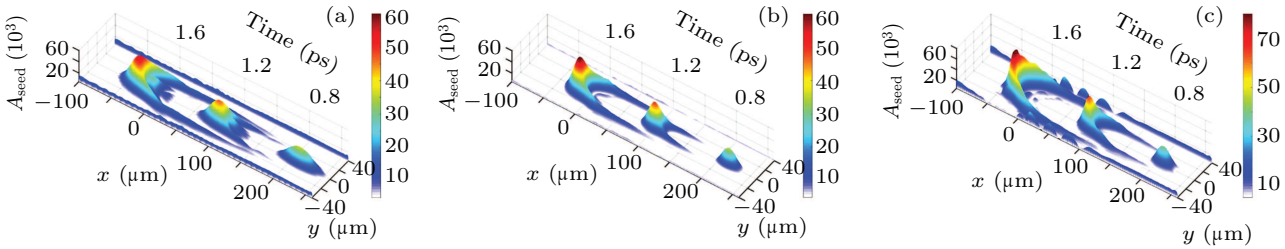


Fig. 9. Evolution of seed amplification at various time in the two-beam amplification. The duration of seed pulse is (a) 100 fs, (b) 50 fs, (c) 50 fs. The seed intensity is 2.0×10^{15} W/cm^2. Each pump intensity is 2.0×10^{14} W/cm^2 in (a), (b), and 4.0×10^{14} W/cm^2 in (c). The amplitude in the z-axis is 1000 times its initial amplitude.

6. Discussion and conclusion

In this paper, we propose a new scheme of multibeam Raman amplification in virtue of the collective mode by sharing a common scattered light. This scheme takes the advantage of larger growth rate through increasing the laser beams, however, this also limits the amplification length. Therefore, we suggest to use a finite-duration seed to facilitate MRA in a short distance. The reason is that finite-duration seed has a real-amplitude growth rate, growing from the original seed amplitude. This growth rate depends on the initial seed amplitude, electron temperature, and seed duration. By using 2D PIC simulations, we have shown that the real-amplitude growth rate of two-beam amplification is much higher than that of the single-beam amplification. An empirical criterion, $\gamma_0 \tau_c = 1$, is used to choose a proper duration for a higher growth rate. Also, the duration has influences on the nonlinear stage of amplification. The two-beam amplification quickly enters the nonlinear stage where pulse compression and a bow shape occur. These nonlinear features indicate that the amplification has come into a self-similar regime.

We have verified the concept of MRA of a finite-duration seed in the short distance regime via two pump beams. The seed pulse grows much faster than the usual BRA scheme, but it has a similar amplification process to that regime. One should note that in our study the pump energy of the two-beam amplification is twice of the single-beam one, and the simulation results show a higher growth rate ratio than the theoretical prediction of $\sqrt{2}$. To make this enhancement clearer, we have performed another single-beam simulation with a doubled pump intensity, 2×10^{14} W/cm^2, so both cases have the same pump energy. The results show that the growth of the two-beam amplification is still higher than that of the single

beam amplification, confirming our conclusion. Finally, we have achieved a higher seed pulse intensity with a fixed amplification length in two-beam amplification, however, it is not a critical intensity that can be obtained by this new scheme. We suggest to achieve higher seed intensity through more laser beams or seed is amplified successively in the overlapping area by the other two overlapping areas extending from this study.

Acknowledgement

We are pleased to acknowledge useful discussions with Qing Jia.

References

[1] Strickland D and Mourou G 1985 *Opt. Commun.* **55** 447
[2] Sadler J D, Silva L O, Fonseca R A, Glize K, Kasim M F, Savin A, Aboushelbaya R, Mayr M W, Spiers B, Wang R H W, Bingham R, Trines R M G M and Norreys P A 2018 *Commun. Phys.* **1** 19
[3] Trines R M G M, Fiuza F, Bingham R, Fonseca R A, Silva L O, Cairns R A and Norreys P A 2011 *Nat. Phys.* **7** 87
[4] Malkin V M, Shvets G and Fisch N J 1999 *Phys. Rev. Lett.* **82** 4448
[5] Malkin V M, Shvets G and Fisch N J 2000 *Phys. Plasmas* **7** 2232
[6] Fisch N J and Malkin V M 2003 *Phys. Plasmas* **10** 2056
[7] Malkin V M and Fisch N J 2005 *Phys. Plasmas* **12** 044507
[8] Shvets G, Fisch N J, Pukhov A and Meyer-ter Vehn J 1998 *Phys. Rev. Lett.* **81** 4879
[9] Trines R M G M, Fiuza F, Bingham R, Fonseca R A, Silva L O, Cairns R A and Norreys P A 2011 *Nat. Phys.* **7** 87
[10] Andreev A A, Riconda C, Tikhonchuk V T and Weber S 2006 *Phys. Plasmas* **13** 053110
[11] Mourou G A, Fisch N J, Malkin V M, Toroker Z, Khazanov E A, Sergeev A M, Tajima T and Le Garrec B 2012 *Opt. Commun.* **285** 720
[12] Capjack C E, James C R and McMullin J N 1982 *J. Appl. Phys.* **53** 4046
[13] Andreev A A and Sutyagin A N 1989 *Sov. J. Quantum Electron.* **19** 1579
[14] Maier M, Kaiser W and Giordmaine J A 1966 *Phys. Rev. Lett.* **17** 1275
[15] Xiao C Z, Zhuo H B, Yin Y, Liu Z J, Zheng C Y, Zhao Y and He X T 2018 *Plasma Phys. Control. Fusion.* **60** 025020
[16] Xiao C Z, Zhuo H B, Yin Y, Liu Z J, Zheng C Y and He X T 2019 *Phys. Plasmas* **26** 062109
[17] Xiao C Z, Zhuo H B, Yin Y, Liu Z J, Zheng C Y and He X T 2020 *Nucl. Fusion* **60** 016022
[18] Jia Q, Barth I, Edwards M R, Mikhailova J M and Fisch N J 2016 *Phys. Plasmas* **23** 053118
[19] Cheng W, Avitzour Y, Ping Y and Suckewer S 2005 *Phys. Rev. Lett.* **94** 045003
[20] Ren J, Cheng W, Li S and Suckewer S 2007 *Nat. Phys.* **3** 732
[21] Ping Y, Kirkwood R K, Wang T L, Clark D S, Wilks S C, Meezan N, Berger R L, Wurtele J, Fisch N J, Malkin V M, Valeo E J, Martins S F and Joshi C 2009 *Phys. Plasmas* **16** 123113
[22] Pai C H, Lin M W, Ha L C, Huang S T, Tsou Y C, Chu H H, Lin J Y, Wang J and Chen S Y 2008 *Phys. Rev. Lett.* **101** 065005
[23] Ren J, Li S, Morozov A, Suckewer S, Yampolsky N A, Malkin V M and Fisch N J 2008 *Phys. Plasmas* **15** 056702
[24] DuBois D F, Bezzerides B and Rose H A 1992 *Phys. Fluids B* **4** 241
[25] Yang S J, Zhuo H B, Yin Y, Liu Z J, Zheng C Y, He X T and Xiao C Z 2020 *Phys. Rev. E* **102** 013205
[26] Balakin A A, Fraiman G M, Fisch N J and Malkin V M 2003 *Phys. Plasmas* **10** 4856
[27] Kirkwood R K, Turnbull D P, Chapman T, Wilks S C, Rosen M D, London R A, Pickworth L A, Dunlop W H, Moody J D, Strozzi D J, Michel P A, Divol L, Landen O L, MacGowan B J, Van Wonterghem B M, Fournier K B and Blue B E 2017 *Nat. Phys.* **14** 80
[28] Jia Q, Shi Y, Qin H and Fisch Nathaniel J 2017 *Phys. Plasmas* **24** 093103
[29] Chen Y, Zheng C Y, Liu Z J, Cao L H, Feng Q S and Xiao C Z 2020 *Plasma Phys. Control. Fusion.* **62** 105020
[30] DuBois D F, Bezzerides B and Rose H A 1992 *Phys. Fluids B* **4** 241
[31] Depierreux S, Neuville C, Baccou C, Tassin V, Casanova M, Masson-Laborde P E, Borisenko N, Orekhov A, Colaitis A, Debayle A, Duchateau G, Heron A, Huller S, Loiseau P, NicolaÏ, Pesme D, Riconda C, Tran G, Bahr R, Katz J, Stoeckl C, Seka W, Tikhonchuk V and Labaune C 2016 *Phys. Rev. Lett.* **117** 235002
[32] Michel P, Divol L, Dewald E L, Milovich J L, Hohenberger M, Jones O S, Hopkins L B, Berger R L, Kruer W L and Moody J D 2015 *Phys. Rev. Lett.* **115** 055003
[33] Edwards M R, Jia Q, Mikhailova J M and Fisch N J 2016 *Phys. Plasmas* **23** 083122
[34] Qu Kenan, Barth Ido and Fisch Nathaniel J 2017 *Phys. Rev. Lett.* **118** 164801
[35] Mounaix P, Pesme D, Rozmus W and Casanova M 1993 *Phys. of Fluids B* **5** 3304
[36] Malkin V M, Shvets G and Fisch N J 2000 *Phys. Rev. Lett.* **84** 1208